

Fermilab

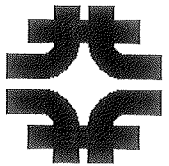
SDC SOLENOID DESIGN NOTE #138

Title: Magnetostatic Analysis of Several SDC Solenoid/Calorimeter Configurations

Author: Bob Wands

Dates: March 22, 1991

Abstract: The position of the SDC calorimetry relative to the coil and the volume of air slots in the calorimetry effect the compressive coil forces and field uniformity. This note studies the effect of nine different calorimetry geometries, and shows that compressive coil forces range from 14 tonnes to 1438 tonnes for the range of parameters considered. Excitation curves and flux plots are also presented for selected configurations.



Magnetostatic Analysis of Several
SDC Solenoid/Calorimeter Configurations

Bob Wands

Introduction

The calorimetry proposed for the SDC experiment provides a solenoid flux return through iron interrupted by air gaps containing scintillator. The purpose of this study is to consider eight calorimeter configurations relative to a solenoid of fixed geometry and the effects on the axial compressive forces on the coil. In addition to these eight cases, the latest available version of the Argonne calorimetry proposal was also evaluated. Field uniformity effects are treated in a separate report by J. Hylen.

Solenoid Parameters

The solenoid is modeled as 8.94 meters long, with a mean radius of 1.81 meters. For the analysis, a radial thickness of 0.02 meters was used, although this is somewhat arbitrary and based mainly on consideration of element aspect ratio for the finite element analysis. A current density of $0.8(10^8)$ amps/m² was used, which provided a central field (@z=0, r=0) of 2 Tesla.

Calorimetry Parameters

A given tower in the calorimeter consists of a repeating pattern of one inch of iron followed by an air gap containing scintillator. The patterns of adjacent towers are staggered as shown in Fig. 1. The towers are everywhere projective relative to the interaction point.

It is known that both the field uniformity and coil forces are strongly dependent on the amount of re-entrant endplug iron, the volume of air in the calorimetry, and the inner radius of the barrel. The test cases varied the geometry of the endplug from a fully re-entrant position 40 cm inside the solenoid bore, to a 'snoutless' version 40 cm outside of the solenoid. The inner radius of the barrel region was varied from 2.28 m to 3 m. The air slot thicknesses were either 1/4 in. or 1/2 in.

Finite Element Model

General

The ANSYS finite element program was used to perform an axisymmetric magnetostatic analysis of the configurations. The formulation is vector potential, and capable of solving for non-linear B-H behaviour. Due to the large number of elements necessary to model the air slots, problems sizes averaged 15000 nodes and elements.

B-H Curves

The small slot size relative to the overall solenoid dimension would require extremely large numbers of nodes and elements if every such slot in the calorimeter were modeled. However, if the direction of the flux within the calorimeter can be assumed to be either all parallel to the long direction of the slot, or all perpendicular to that direction, then B-H approximations can be made which allow the iron and slots to be 'smeared' into a homogeneous material.

The assumption of uniform direction is not realistic in the endplug region of the calorimeter, since it is within this region that the flux must wrap radially around the end of the solenoid to reach the barrel. In this region, each slot and plate were modeled with finite elements.

In the barrel region, the flux can be assumed to be parallel to the long slot direction. In this case, it is known from Maxwell's equations that the parallel component of H in the air must equal the parallel component of H in the iron. So, a B-H curve can be constructed by using the value of H for iron, and calculating the corresponding value of B by taking the area-weighted average of the B-field in the iron and air.

$$H = H_{\text{iron}}$$

$$B = B_{\text{iron}}(t_i/(t_i+t_a)) + B_{\text{air}}(t_a/(t_i+t_a))$$

where t_i = thickness of iron plate
 t_a = thickness of air slot

The iron B-H curve used was a curve for 1020 steel measured for the CDF solenoid.

Results

Axial Compressive Forces

The axial force on the coil due to the interaction of the current sheet with the radial field components was calculated within the ANSYS program from the current density and field solution for each of the nine test cases, and is shown in Fig. 2. Test case 5, which has the endplug at its greatest distance from the coil and the barrel region as close as possible, gives the largest compressive coil force of 1140 tonnes. This is because the flux is encouraged to turn around the end of the solenoid to reach the barrel, providing a large radial field component.

The smallest axial force is found in test case 4, which has the endplug brought flush with the end of the current sheet. This is a physically impossible configuration, due to the need for a cryostat around the superconducting coil, but it illustrates the ability of the endplug to keep the flux oriented axially past the end of the current sheet.

This ability is confirmed by the flux plots for several cases shown in Fig. 3. The re-entrant endplugs can effectively combine a realistic configuration with the ability to keep radial field components small. The flux plots also confirm qualitatively that the configurations with large axial compressive forces are also those with the most non-uniform field distributions at the solenoid ends.

Excitation Curves

Test cases 0,2,7 and 8 were run for three different current densities to look at saturation effects on the axial coil forces. Fig. 4 shows that test case 2, with both the endplug and barrel at their maximum distance from the current sheet, and test case 8, with 1/2 in air slots, give the largest compressive forces. Test cases 0 and 7, with long re-entrant endplug sections, show a tendency to actually stretch the coil under small excitations. This is due to flux bending toward the highly permeable re-entrant section and causing the radial field component to reverse slightly. At higher excitations, the endplug becomes less permeable and the flux assumes the more natural tendency to bend outward toward the barrel region.

The Argonne Geometry

In addition to the test cases 0-8, the latest configuration available for the Argonne version of the calorimetry was also modeled. The geometry, based on a drawing dated 3-12-91, and the resulting axial forces are shown in Fig. 5. This geometry uses a shorter solenoid than was assumed for test cases 0-8, and places the slotted calorimetry at a greater distance from the current sheet, due to the use of a large lead EM section. The resulting axial force of 1438 tonnes is the largest of any configuration, as would be expected from the calorimetry placement. A flux plot, shown in Fig. 6, shows that substantial flux return occurs in the air around the solenoid end, resulting in the large forces, as well as a highly non-uniform field near the end of the solenoid.

Conclusions

This study provides an estimate of the effects of several calorimeter configurations on the coil forces and field uniformity. General findings are that designs with low forces and uniform fields require that endplug to be as close as practical to the end of the current sheet, and even re-entrant if possible. The inner radius of the barrel region is less important. The fraction of air in the calorimetry is a major factor, but the 1/4 ratio of air to iron assumed for most test cases is probably realistic.

MARSY8 1994A
12:01:55
PLOT NO. 1
PREP7 ELEMENTS
TYPE NUM

ZV =1
*DIST=0.340096
*XF =1.719
*YF =-4.571
EDGE

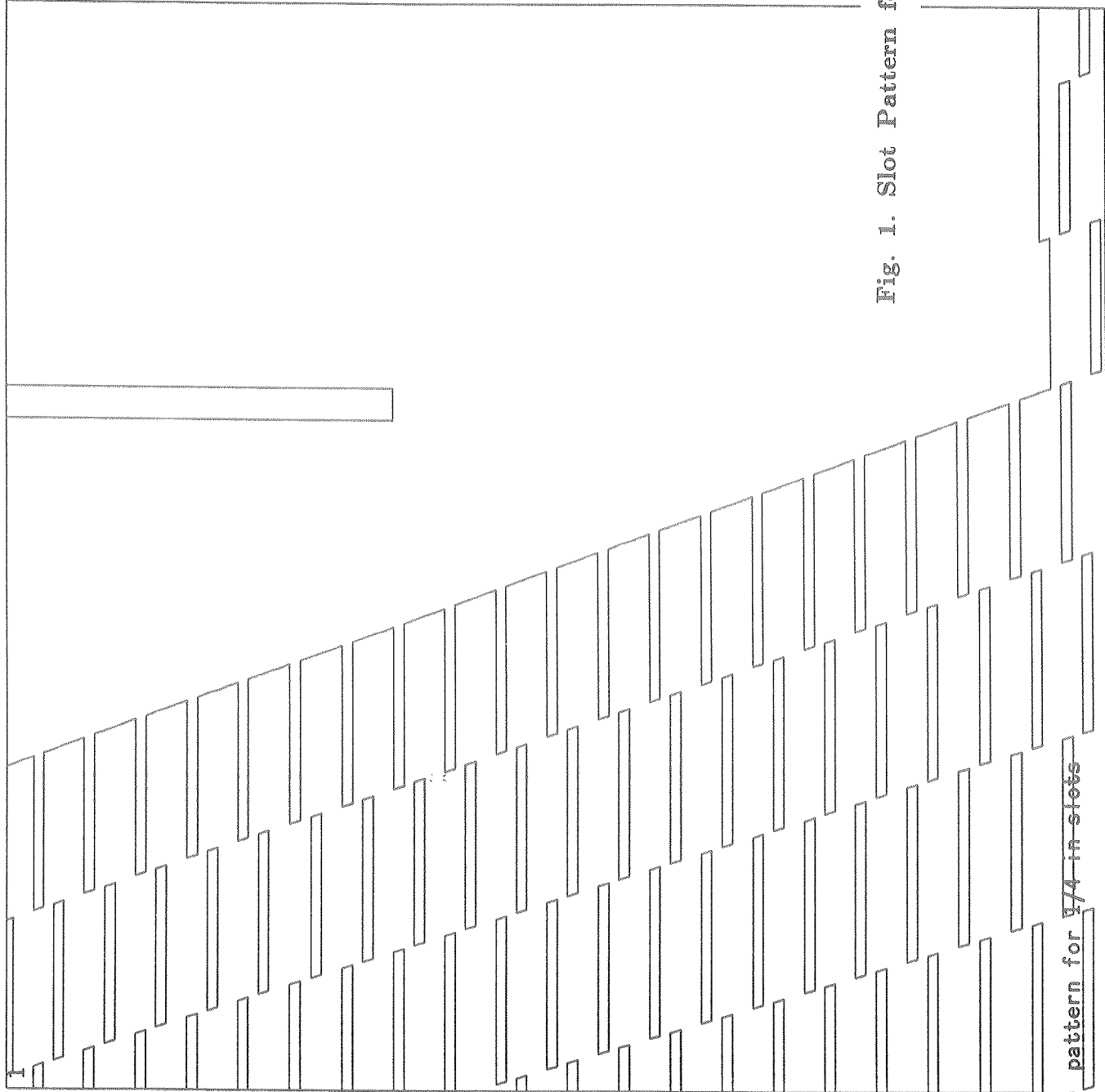


Fig. 1. Slot Pattern for Calorimetry

pattern for 1/4-in slots

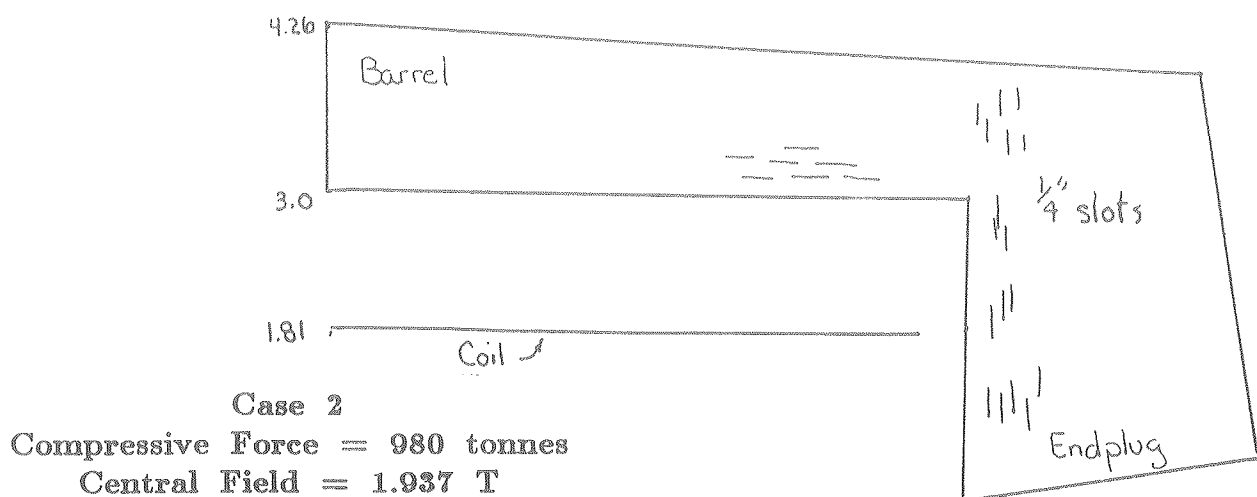
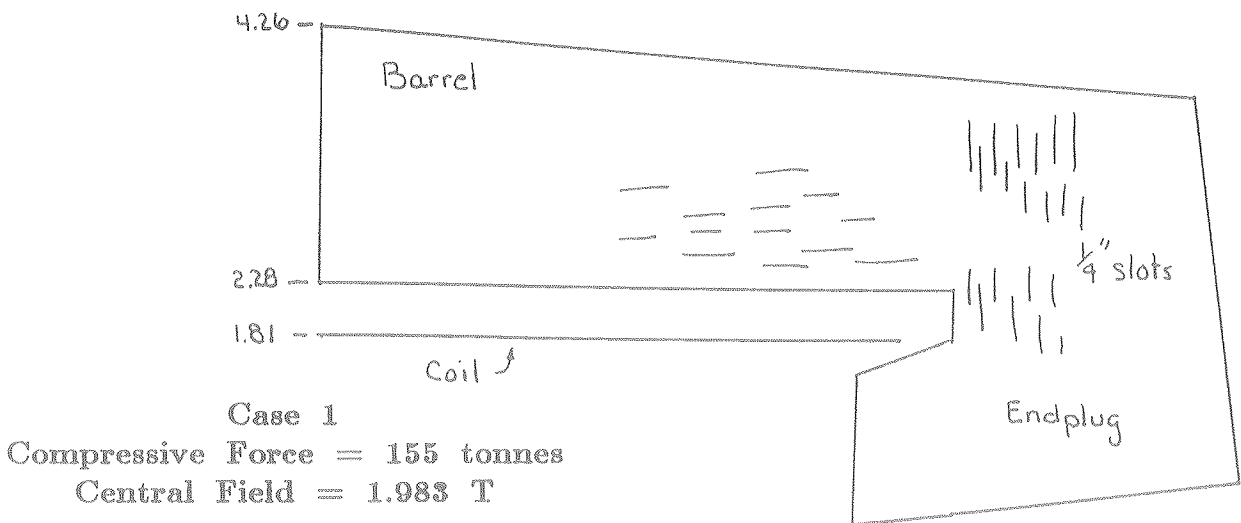
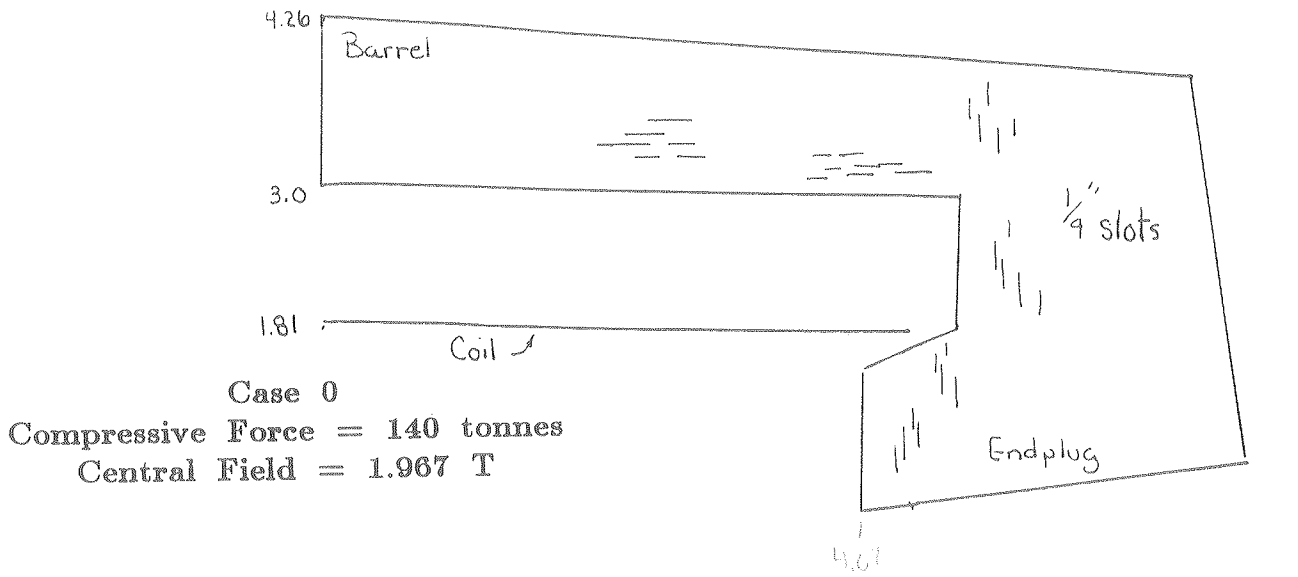
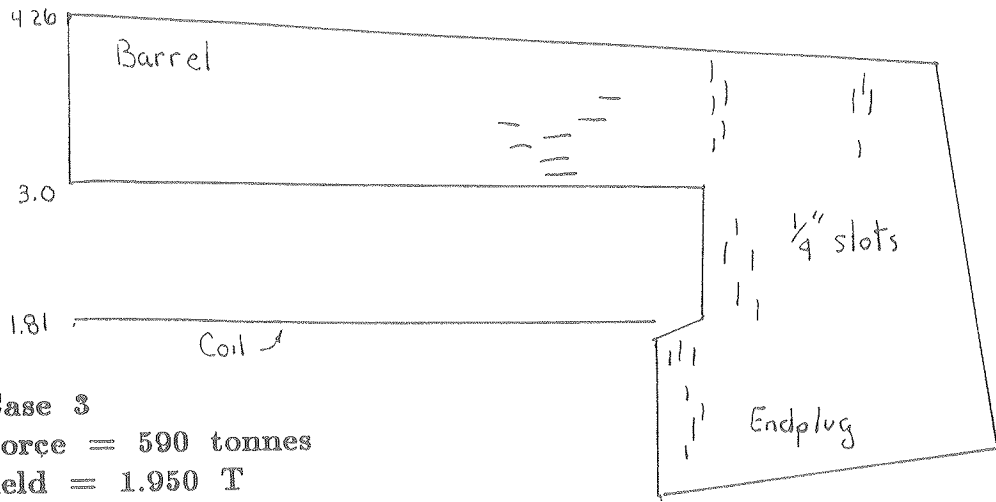
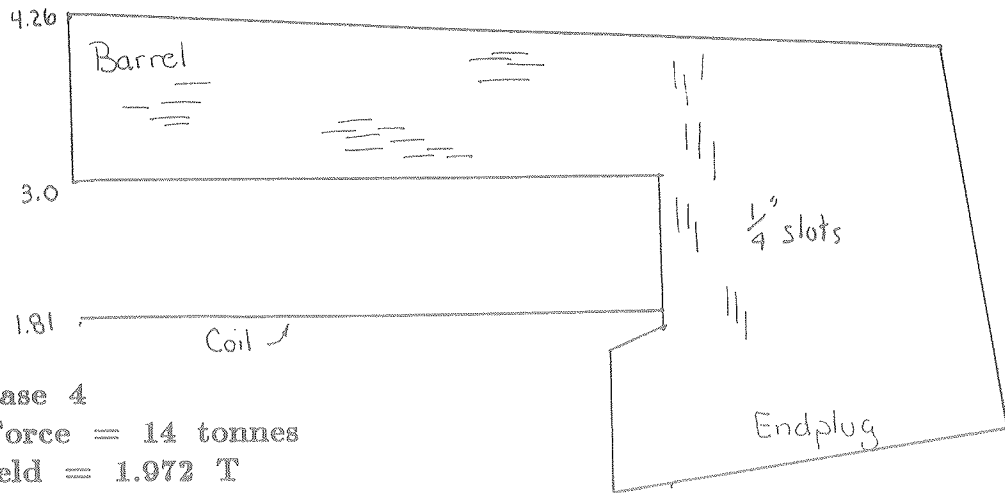


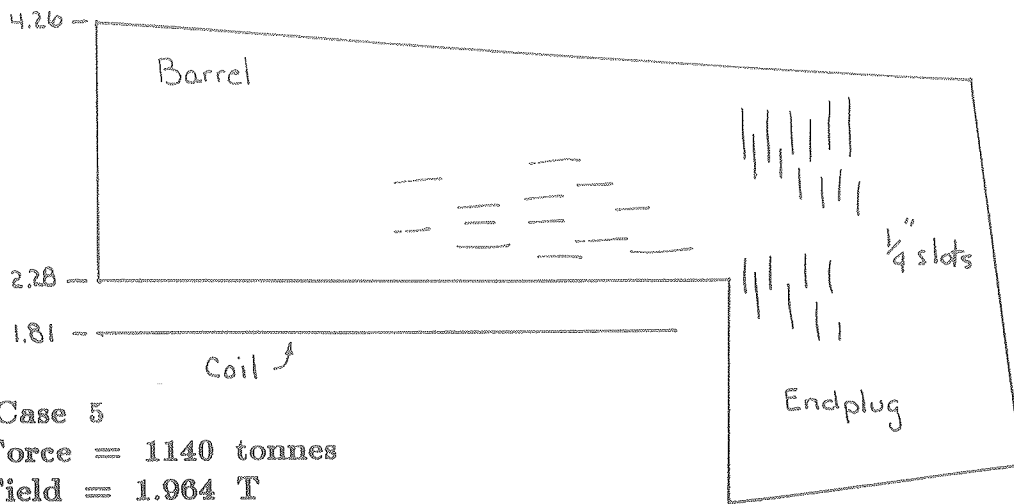
Fig. 2. Axial Compressive Forces on Coil



Case 3
 Compressive Force = 590 tonnes
 Central Field = 1.950 T



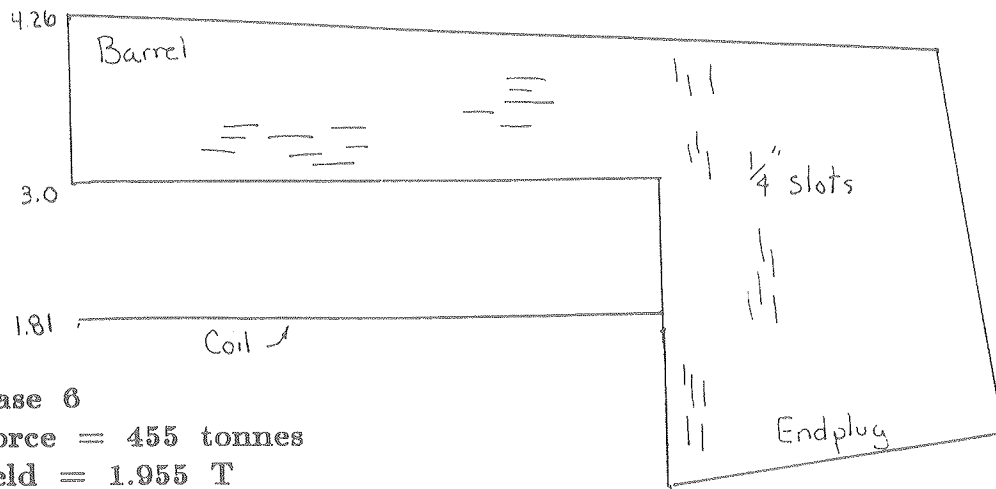
Case 4
 Compressive Force = 14 tonnes
 Central Field = 1.972 T



Case 5
 Compressive Force = 1140 tonnes
 Central Field = 1.964 T



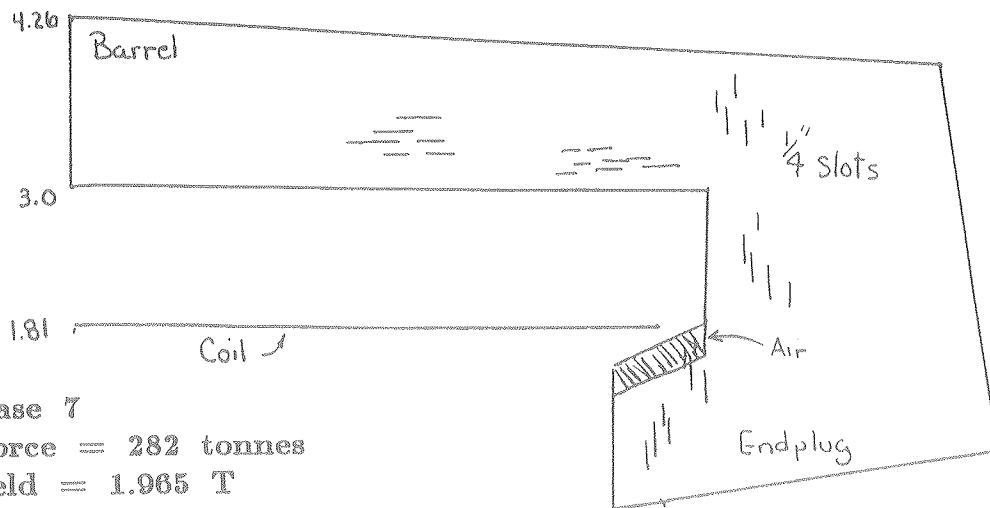
Fig. 2. (cont'd)



Case 6

Compressive Force = 455 tonnes

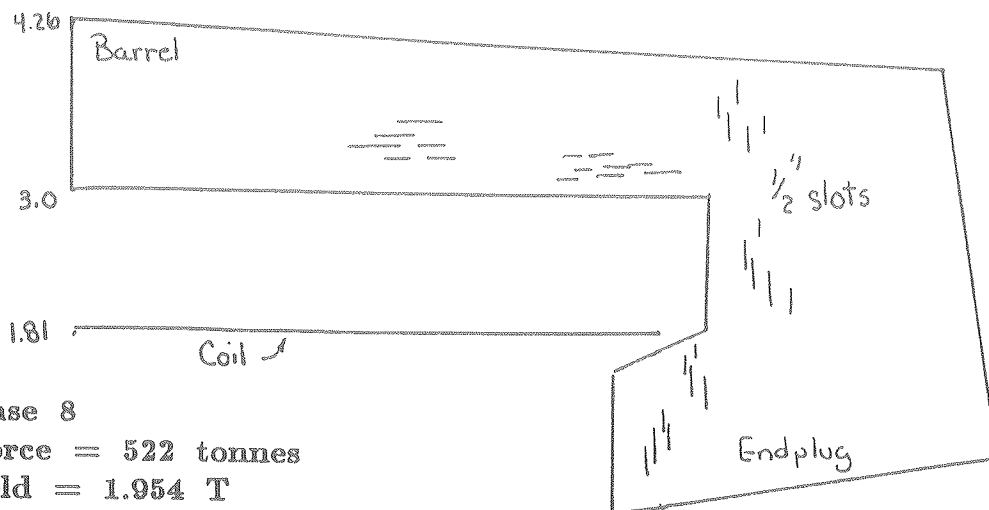
Central Field = 1.955 T



Case 7

Compressive Force = 282 tonnes

Central Field = 1.965 T



Case 8

Compressive Force = 522 tonnes

Central Field = 1.954 T



Fig. 2. (cont'd)

1
MANSYS 1994A
8:12:32
PLOT NO. 1
POST1 VECTOR
STEP=1
ITER=1
BMAG
ELEM=857
0.281065
0.561975
0.842885
1.124
1.405
1.686
1.967
2.247
2.528
ZV =1
DIST=3.894
XF =2.13
YF =-3.54
EDGE

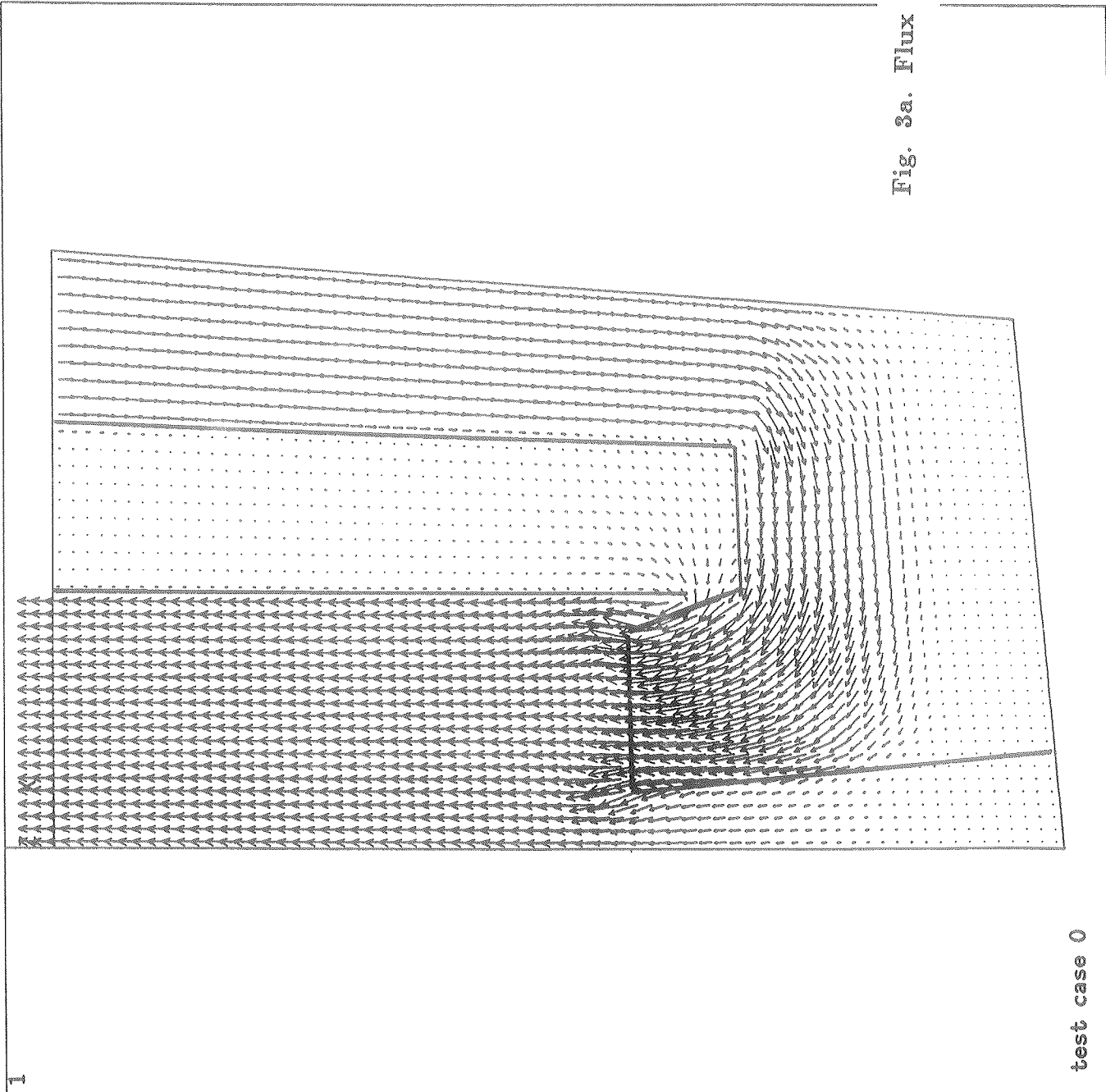


Fig. 3a. Flux Plot for Test Case 0

test case 0

MANYS18 1991A
7:17:47
PLOT NO. 1
POST1 VECTOR
STEP=1
ITER=1
BMAG
ELEM=857
0.28302
0.565899
0.848779
1.132
1.415
1.697
1.98
2.263
2.546
ZV =1
DIST=3.894
XF =2.13
YF =-3.54
EDGE

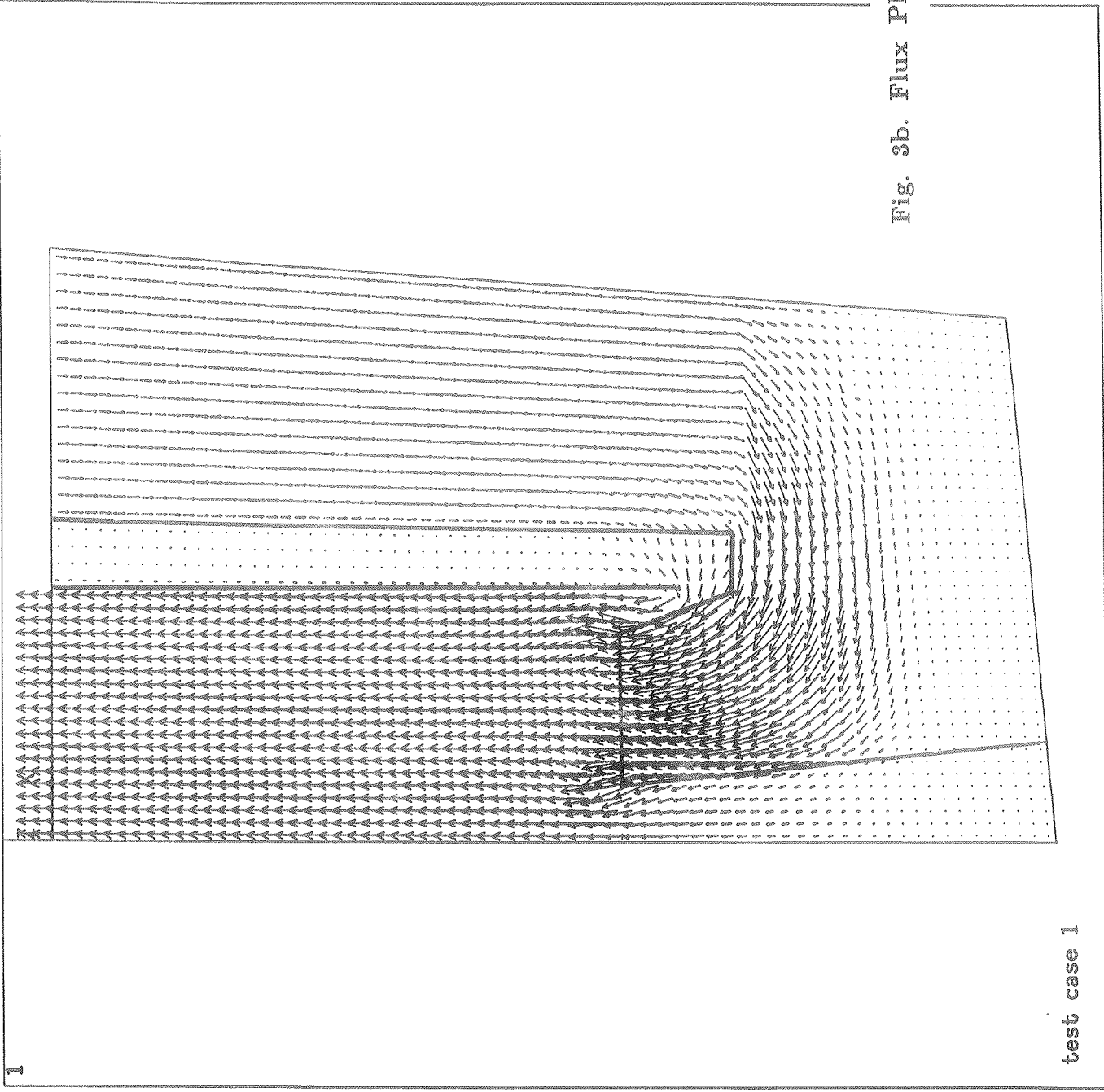


Fig. 3b. Flux Plot for Test Case 1

test case 1

MANSYS 1991A
8:28:35
PLOT NO. 1
POST1 VECTOR
STEP=1
ITER=1
BMAG
ELEM=20
0.219527
0.43903
0.658532
0.878035
1.098
1.317
1.537
1.756
1.976
ZV =1
DIST=3.894
XF =2.13
YF =-3.54
EDGE

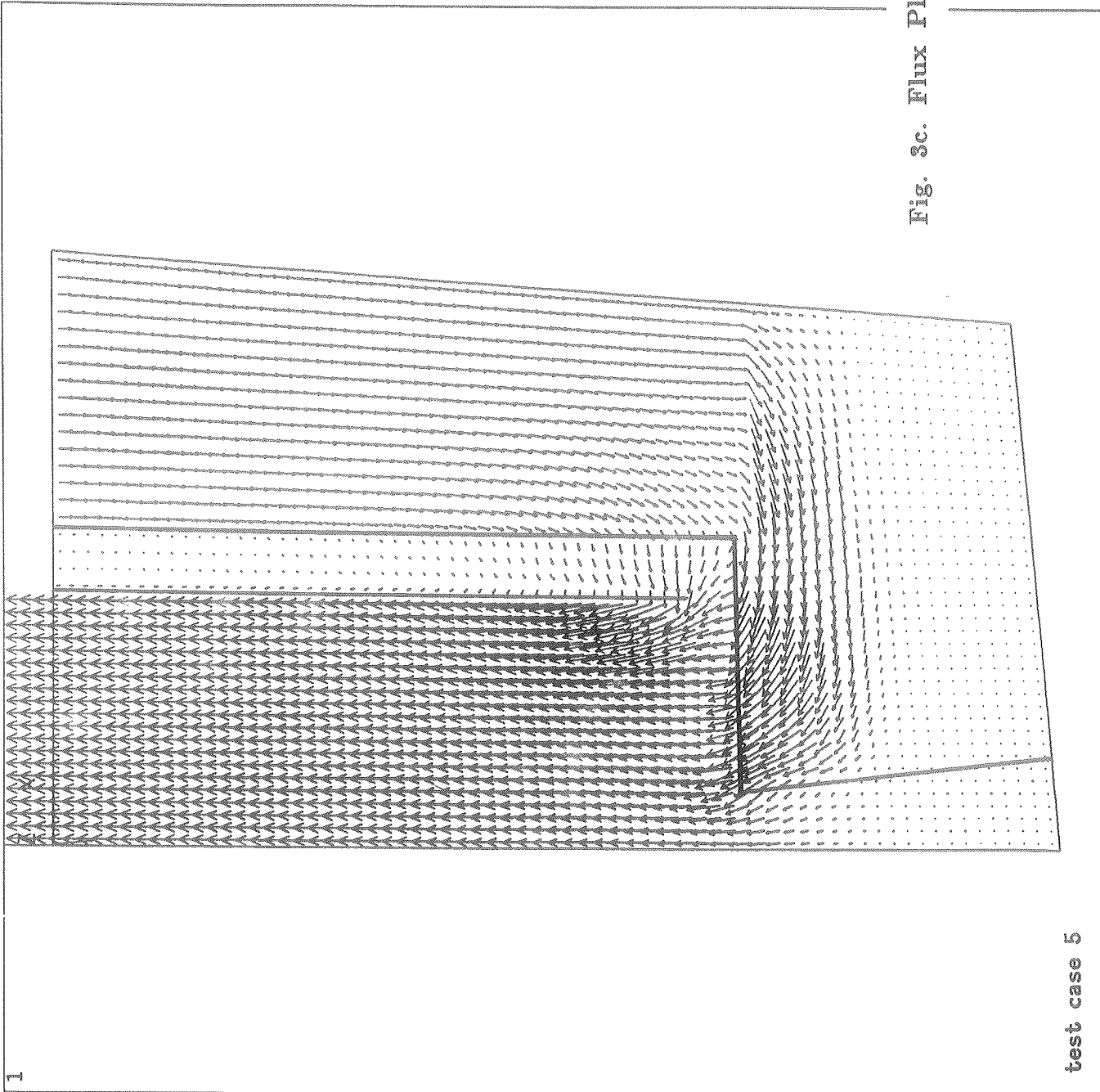


Fig. 3c. Flux Plot for Test Case 5

test case 5

MANSYS 1994A
7:52:48
PLOT NO. 1
POST1 VECTOR
STEP=1
ITER=1
BMAG
ELEM=856
0.28124
0.562332
0.843424
1.125
1.406
1.687
1.968
2.249
2.53

ZV =1
DIST=3.894
XF =2.13
YF =-3.54
EDGE

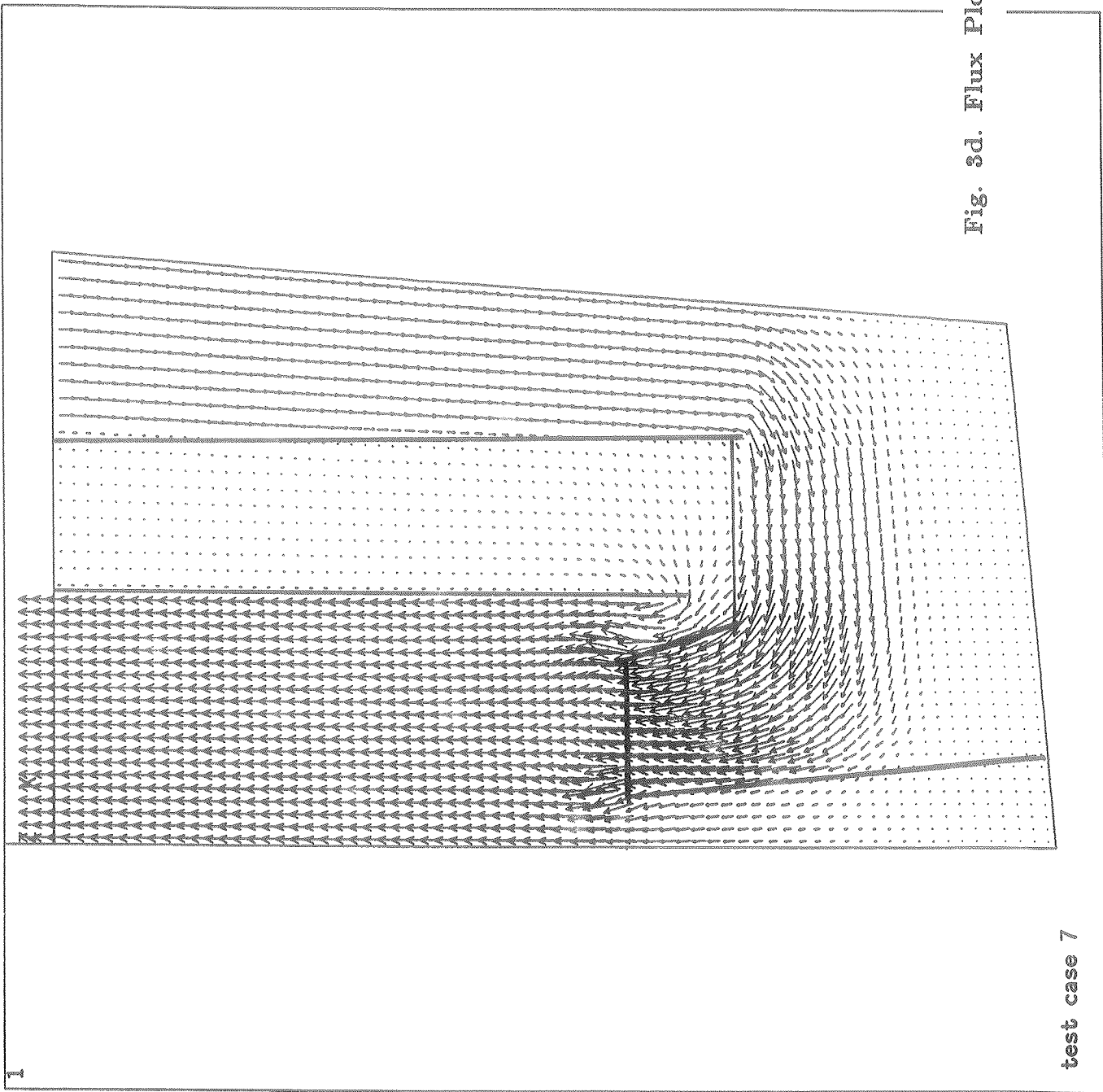
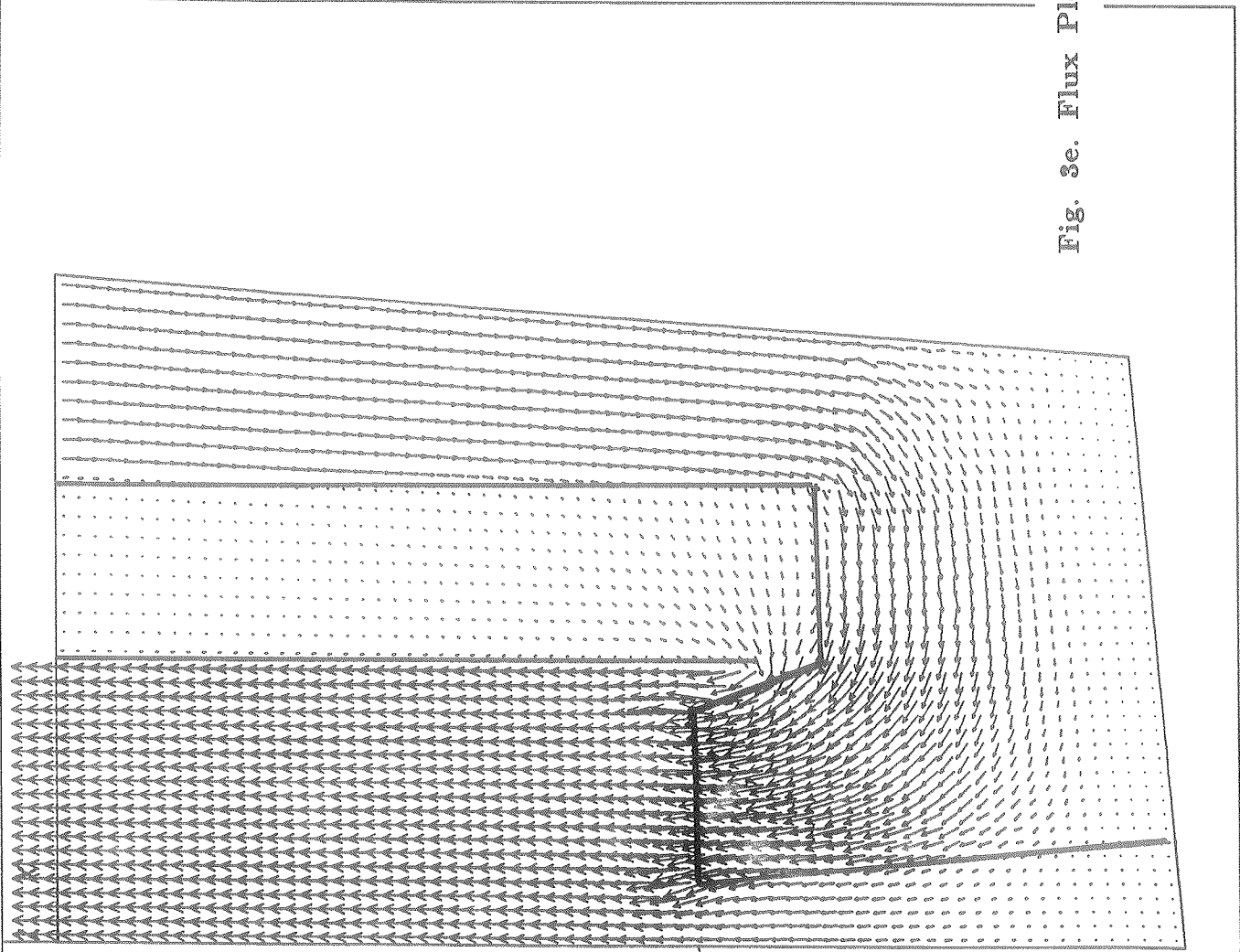


Fig. 3d. Flux Plot for Test Case 7

test case 7

1
MANSYS 1994A
7:51:01
PLOT NO. 1
POST1 VECTOR
STEP=1
ITER=1
BMAG
ELEM=857
0.250926
0.501198
0.751471
1.002
1.252
1.502
1.753
2.003
2.253
ZV =1
DISI=3.894
XF =2.13
YF =-3.54
EDGE



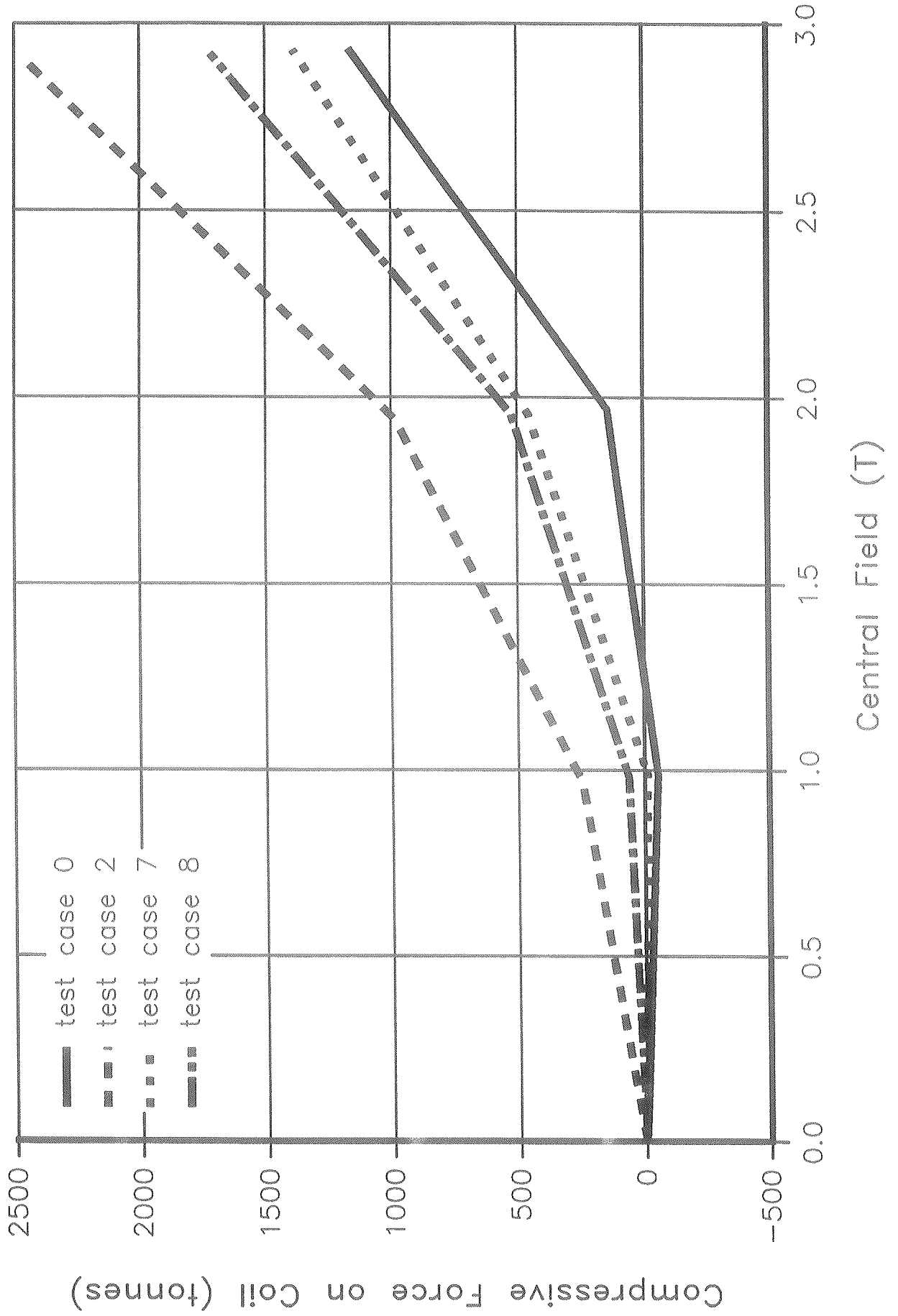
test case 8

Fig. 3e. Flux Plot for Test Case 8

Fig. 4. Excitation Curves

Axial Compressive Force on Coil vs Central Field

comparison of four test cases



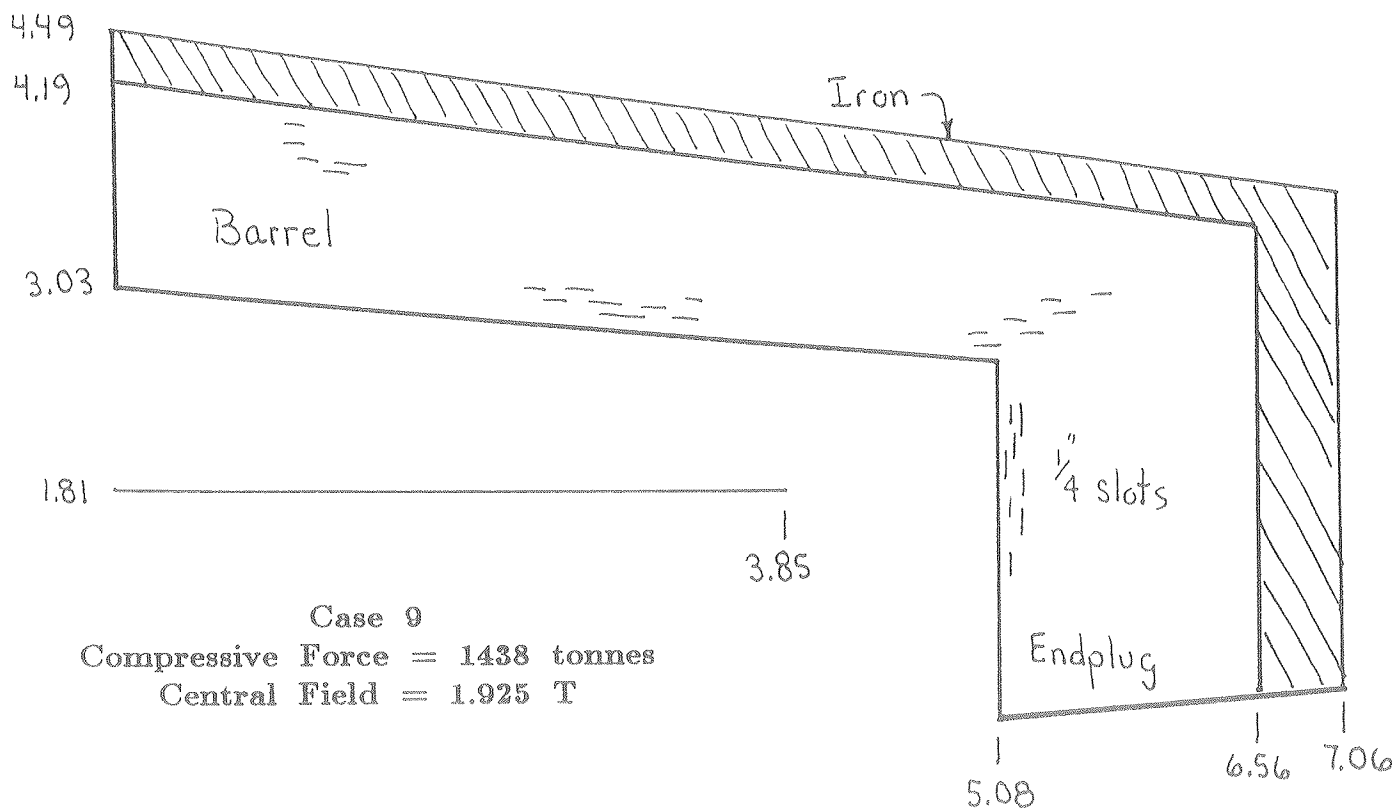


Fig. 5. Compressive Force on Coil for Argonne Geometry

```

ANSYS 4.4A
MAR 19 1991
15:11:08
PLOT NO. 1
POST1 VECTOR
STEP=1
ITER=1
BMAG
ELEM=20
Ø.21804
Ø.435648
Ø.653257
Ø.870865
1.088
1.306
1.524
1.741
1.959

ZV =1
DIST=3.884
XF =2.244
YF =-3.531
EDGE

```

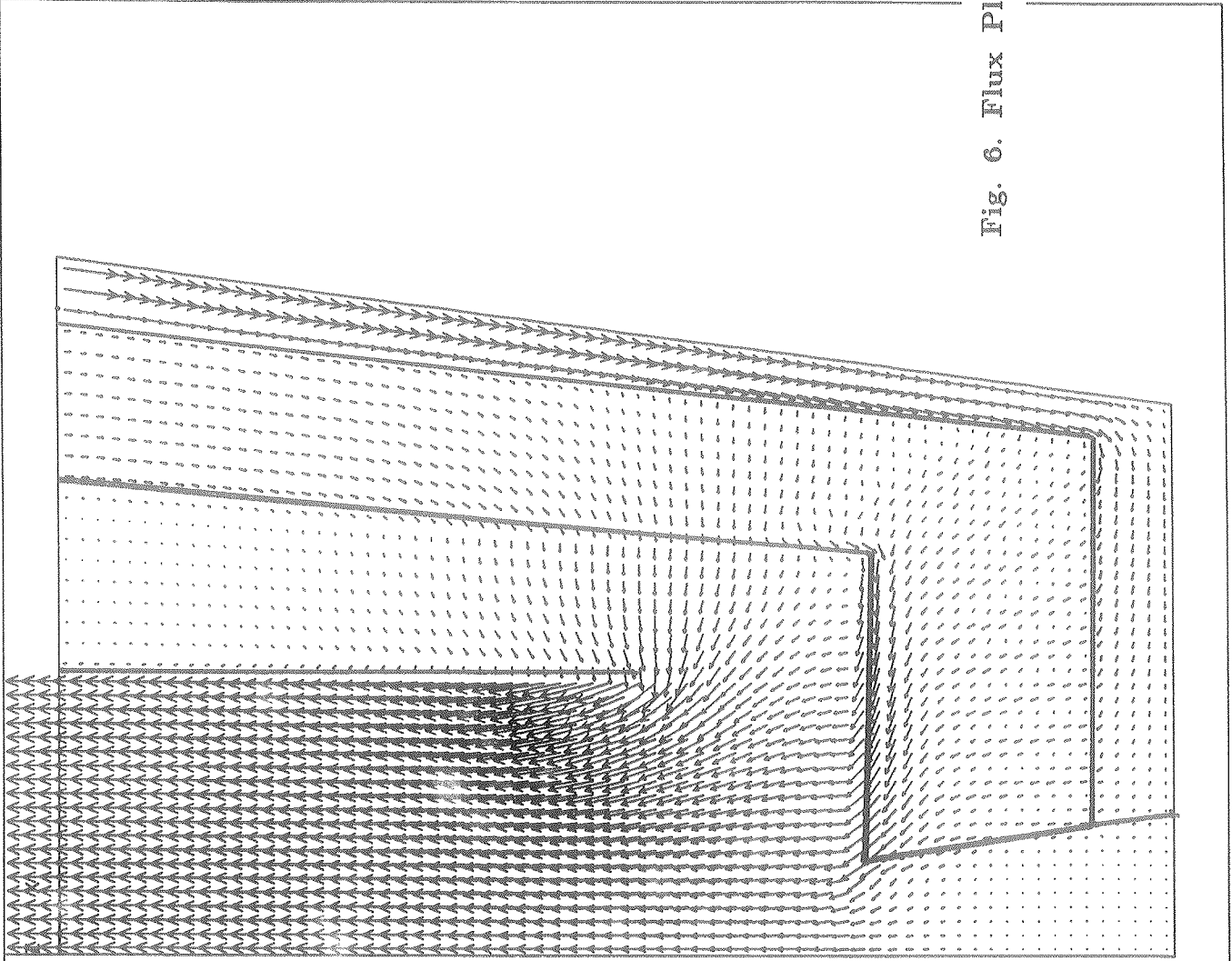


Fig. 6. Flux Plot for Argonne Geometry